Topological phase in a Kitaev chain with spatially separated pairing processes

Y. B. Shi and Z. Song*
School of Physics, Nankai University, Tianjin 300071, China

(Received 15 November 2022; revised 20 February 2023; accepted 23 February 2023; published 3 March 2023)

The dynamic balance between pair creation and annihilation processes takes a crucial role to the topological superconductivity in the Kitaev model. Here we study the effect of spatial separation of creation and annihilation terms, i.e., sources and drains of pair are arranged alternatively. In this regard, a non-Hermitian Hamiltonian is naturally considered, which may possess complex energy branches. However, when the Bardeen-Cooper-Schrieffer pair excitation is only considered, the spectrum in such a subspace is fully real. In particular, the Zak phases extracted from the pair wave function are quantized and therefore able to characterize the different phases regardless of the breaking of time-reversal symmetry. For open chain system, the corresponding Majorana lattice is investigated. We find that although there are complex modes, all the edge modes have zero energy and obey the bulk-boundary correspondence. This results in the Kramer-type degeneracy of both the real and complex levels as a signature of the topologically nontrivial phase.

DOI: 10.1103/PhysRevB.107.125110

I. INTRODUCTION

In traditional quantum mechanics, the fundamental postulate of the Hermiticity of the Hamiltonian ensures the reality of the spectrum and the unitary dynamics for a closed quantum system [1]. In general, any Hermitian Hamiltonian can also be decomposed into two non-Hermitian sub-Hamiltonians which are Hermitian conjugates of each other. There are many different ways of decomposing a Hamiltonian. In this sense, the reality of spectrum roots in the balance of the actions of the two non-Hermitian sub-Hamiltonians. Intuitively, the Hermiticity is not necessary for the balance. In fact, this postulate has been questioned by the existence of entirely real spectra of a certain class of non-Hermitian Hamiltonians [2,3]. Such kinds of Hamiltonians, referred to as pseudo-Hermitian operator [4–8], possess a particular symmetry, i.e., it commutes with the combined operator $\mathcal{PT}$, but not necessarily with $\mathcal{P}$ and $\mathcal{T}$ separately. Here $\mathcal{P}$ is a unitary operator, such as parity, translation, rotation operators, etc., while $\mathcal{T}$ is an antiunitary operator, such as time-reversal operator. The combined symmetry is said to be unbroken if every eigenstate of the Hamiltonian is $\mathcal{PT}$ symmetric and the entire spectrum is real; it is said to be spontaneously broken if some eigenstates of the Hamiltonian are not the eigenstates of the combined symmetry. Such a symmetry can be regarded as a demonstration of the balance, for instance, a simple gain-loss–balanced system in Refs. [9–11]. This concept should be extended to a system without conservation of particle number.

The Kitaev model is a typical one for violating particle conservation. It is believed to capture the feature of one-dimensional topological superconductor for spinless fermions with p-wave pairing [12]. The topological superconducting phase has been demonstrated by unpaired Majorana modes exponentially localized at the ends of open Kitaev chains [13–15]. Intimately related to the superconducting phase, the dynamic balance between pair creation and annihilation processes takes a crucial role, which violates the conservation of the fermion number but preserves its parity. It is the fermionized version of the familiar one-dimensional transverse-field Ising model [16], which is one of the simplest solvable models exhibiting quantum criticality and demonstrating a quantum phase transition with spontaneous symmetry breaking [17]. So far, most of the investigations on the Kitaev model have focused on the case with the balanced pair creation and annihilation at the same location, as pair source and drain, respectively. In principle, there are many other types of balance between pair creation and annihilation such as the sources and drains of pair are arranged alternatively (Fig. 1). Intuitively, such kinds of balance should take the similar role in the existence of the gapped superconducting phase. However, when these cases are considered, the traditional method is no longer valid because a non-Hermitian Hamiltonian is involved.

The strategy of this paper is to study the topological phase in Kitaev chain with spatially separated pairing processes based on the non-Hermitian quantum theory. Non-Hermitian Kitaev models [18–26] and Ising models [27–30] have been studied within the pseudo-Hermitian framework. Also, the experimental schemes for realizing the Kitaev model and related non-Hermitian systems have been presented in Refs. [31,32], respectively. In this work, we study the effect of spatial separation of creation and annihilation terms, i.e., sources and drains of pair are arranged alternatively. It is a non-Hermitian model with time-reversal symmetry, rather than a combined $\mathcal{PT}$ symmetry. Exact solution shows a rich phase diagram, including gapped superconducting phases associated with both time-reversal symmetry and broken time-reversal symmetry. However, when only the Bardeen-Cooper-Schrieffer (BCS-type) pair excitation is considered, the spectrum in

*songtc@nankai.edu.cn

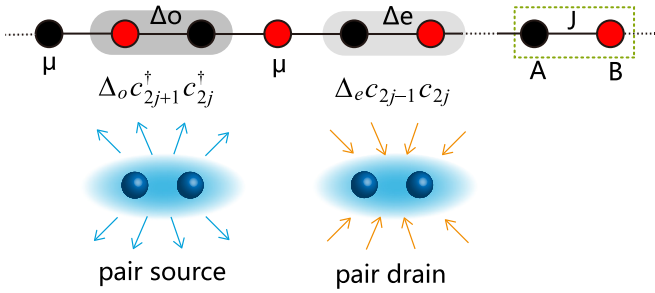

FIG. 1. (a) Schematic of the 1D Kitaev model for spinless fermion with non-Hermitian imbalanced pair terms, arising from specially separated creation and annihilation. Here J is the hopping strength between two adjacent sites and the dark (light) shade region represents the pair creation (annihilation) on odd (even) dimer with amplitude Δ_o (Δ_e). The staggered pair terms describe the source and drain of nearest-neighboring fermion pairs. The unit cell consists of two sublattices A and B in black and red as indicated inside the dashed green rectangle. μ is the chemical potential.

the subspace is fully real. There are two topological superconducting phases characterized by the extended Zak phase, which is defined in terms of biorthonormal inner product [33,34]. The Zak phases extracted from the pair wave function are quantized and therefore able to characterize the different phases regardless of the breaking of time-reversal symmetry. We also investigate the bulk-edge correspondence in such a non-Hermitian system via the Majorana transformation. The corresponding Majorana lattice for open chain system is investigated. We find that although there are complex modes, all the edge modes have zero energy and obey the bulk-edge correspondence. This results in the Kramer-type degeneracy of both the real and complex levels as a signature of the topologically nontrivial phase.

In comparison with the original Kitaev chain, the present non-Hermitian Kitaev chain remains the topological phase, which can be identified by the Zak phase, two types of order parameters, in the context of biorthonormal inner product. In addition, the bulk-boundary correspondence still holds although the Majorana lattice is non-Hermitian. However, on the other hand, the spectrum becomes complex in the symmetry-breaking region, but keeping the reality of the pair spectrum. We also find that the phase boundary is independent of the symmetry-breaking region, but dependent of the strength of the pair term.

This paper is organized as follows. In Sec. II, we describe the model Hamiltonian and present the solutions. In Sec. III, we investigate the phase diagram and analyze the signatures of the phase boundary based on the solutions. In Sec. IV we construct the pair wave function and calculate the Zak phase to discuss the topological properties of the system. In Sec. V, we study the corresponding Majorana lattice to show the existence of the bulk-edge correspondence. In Sec. VI we provide the implication of the zero modes. Finally, we give a summary and discussion in Sec. VII. Some details of derivations are placed in the Appendix.

II. MODEL AND PAIR SPECTRUM

We consider the following fermionic Hamiltonian on a lattice of length $2N$:

$$H = \sum_{l=1}^{2N} [J c_l^\dagger c_{l+1} + \text{H.c.} + \mu(1-2n_l)] + \sum_{j=1}^{N} (e^{i\varphi}\Delta_o c^\dagger_{2j+1} c^\dagger_{2j} + e^{-i\varphi}\Delta_e c_{2j-1} c_{2j}), \quad (1)$$

where $c_l^\dagger$ (c_l) is a fermionic creation (annihilation) operator on site l, $n_l = c_l^\dagger c_l$, J the tunneling rate, μ the chemical potential, and real number Δ_o (Δ_e) the strength of the p-wave pair creation (annihilation) on odd (even) dimer. For a closed chain, we define $c_{2N+1} = c_1$ and for an open chain, we set $c_{2N+1} = 0$. The Kitaev model is known to have a rich phase diagram in its Hermitian version, i.e., $H \to H + H^\dagger$.

Comparing with the non-Hermitian Kitaev model in previous works [18–26], the present model has time-reversal symmetry and its non-Hermiticity arises from the staggered unidirectional pairing term, which has never been reported in the literatures. The physical intuition for this modification is simple. It is the simplest model to characterize the system with nonlocally pairing processes, i.e., the pair creation and annihilation occurring at different dimers.

In this work, we only consider the reduced Hamiltonian by taking $\Delta_o = \Delta_e = \Delta > 0$ and $\varphi = 0$. Mathematically, the reduced and the original Hamiltonians can be mapped from one to another via a local transformation. Actually, taking the similarity transformation

$$c_j = e^{-\gamma/2} e^{-i\varphi/2} c_j, \quad \bar{c}_j = e^{\gamma/2} e^{i\varphi/2} c_j^\dagger, \quad (2)$$

with $e^\gamma = \Delta_o/\Delta_e$ and $\Delta = \sqrt{\Delta_o \Delta_e}$, one can get the reduced Hamiltonian with the operators $H(c_j, \bar{c}_j)$. Note that operators $(c_j, \bar{c}_j)$ satisfy the canonical relations

$$\{c_i, \bar{c}_j\} = \delta_{ij}, \quad \{c_i, c_j\} = \{\bar{c}_i, \bar{c}_j\} = 0, \quad (3)$$

and then any two Hamiltonians $H(c_i, \bar{c}_j)$ and $H(c_i, c_j^\dagger)$ have the same structure of the solution [24], sharing similar features.

Before solving the Hamiltonian (reduced Hamiltonian with $\Delta_o = \Delta_e = \Delta > 0$ and $\varphi = 0$), it is profitable to investigate the symmetry of the system and its spontaneous breaking in the eigenstates. It can be checked that the model respects two evident symmetries. The first one is the parity symmetry

$$[\Pi, H] = 0, \quad (4)$$

where the parity operator about fermion number is defined as $\Pi = \prod_{j=1}^{N} (-1)^{n_j}$. Second, by the direct derivation, we have $[\mathcal{T}, H] = 0$, i.e., the Hamiltonian is a time-reversal ($\mathcal{T}$) invariant, where the antilinear time-reversal operator $\mathcal{T}$ has the function $\mathcal{T} i \mathcal{T} = -i$. In general, the $\mathcal{T}$ symmetry in a non-Hermitian model plays the same role as the $\mathcal{PT}$ symmetry, probably resulting a $\mathcal{PT}$ pseudo-Hermitian system. It motivates a more systematic study of such a model, including the influence of the spontaneous breaking to the topological phase.

We introduce the Fourier transformations in two sublattices

$$c_j = \frac{1}{\sqrt{N}} \sum_k e^{ikn} \begin{cases} \alpha_k, & j = 2n \\ \beta_k, & j = 2n-1 \end{cases} \tag{5}$$

where $n = 1, 2, \ldots, N$, $k = 2m\pi/N$, $m = 0, 1, 2, \ldots, N-1$. Inversely, the spinless fermionic operators in k space α_k, β_k are

$$\begin{cases} \alpha_k = \frac{1}{\sqrt{N}} \sum_j e^{-ikn} c_j, & j = 2n \\ \beta_k = \frac{1}{\sqrt{N}} \sum_j e^{-ikn} c_j, & j = 2n-1. \end{cases} \tag{6}$$

The Hamiltonian with periodic boundary condition can be block diagonalized by this transformation due to its translational symmetry, i.e.,

$$H = \sum_{k\in(0,\pi]} H_k = \psi_k^\dagger h_k \psi_k, \tag{7}$$

satisfying $[H_k, H_{k'}] = 0$, where the operator vector $\psi_k^\dagger = (\alpha_k^\dagger \quad \beta_k^\dagger \quad \alpha_{-k} \quad \beta_{-k})$, and the core matrix

$$h_k = \begin{pmatrix} -2\mu & \gamma_k & 0 & -\Delta e^{ik} \\ \gamma_k^* & -2\mu & \Delta e^{-ik} & 0 \\ 0 & -\Delta & 2\mu & -\gamma_k \\ \Delta & 0 & -\gamma_k^* & 2\mu \end{pmatrix}, \tag{8}$$

with $\gamma_k = J(1 + e^{ik})$. So far the procedure is the same as that for solving a Hermitian Hamiltonian. Obviously, matrix h_k is no longer Hermitian. To diagonalize a non-Hermitian Hamiltonian, one should introduce the Bogoliubov transformation in the complex version:

$$A^k_{\rho\sigma} = (V^k \psi_k)_{\rho\sigma}, \quad \overline{A}^k_{\rho\sigma} = (\psi_k^\dagger \overline{V}^k)_{\rho\sigma}, \tag{9}$$

with $\rho, \sigma = \pm$, where V^k and $\overline{V}^k = (V^k)^{-1}$ are similarity transformation for the diagonalization of h_k, i.e.,

$$V^k h_k \overline{V}^k = \mathrm{dia}(\varepsilon^k_{++} \quad \varepsilon^k_{+-} \quad \varepsilon^k_{--} \quad \varepsilon^k_{-+}). \tag{10}$$

In the Appendix, Sec. A 1, the explicit form of V^k and $\overline{V}^k$ is presented. This procedure essentially establishes the biorthogonal basis, which is a crucial step to solve a pseudo-Hermitian Hamiltonian. Obviously, complex Bogoliubov modes $(A^k_{\rho\sigma}, \overline{A}^k_{\rho\sigma})$ satisfy the anticommutation relations

$$\{A^k_{\rho\sigma}, \overline{A}^{k'}_{\rho'\sigma'}\} = \delta_{kk'}\delta_{\rho\rho'}\delta_{\sigma\sigma'}, \tag{11}$$

$$\{A^k_{\rho\sigma}, A^{k'}_{\rho'\sigma'}\} = \{\overline{A}^k_{\rho\sigma}, \overline{A}^{k'}_{\rho'\sigma'}\} = 0, \tag{12}$$

which result in the diagonal form of the Hamiltonian

$$H = \sum_k \sum_{\rho,\sigma=\pm} \varepsilon^k_{\rho\sigma} \overline{A}^k_{\rho\sigma} A^k_{\rho\sigma}. \tag{13}$$

Here the dispersion relation of the quasiparticle is given by

$$\varepsilon^k_{\rho\sigma} = \rho\sqrt{\Lambda_k + \sigma\sqrt{\Omega_k}}, \tag{14}$$

where

$$\Lambda_k = 4\mu^2 + 4J^2\cos^2\frac{k}{2} - \Delta^2\cos k, \tag{15}$$

$$\Omega_k = 64\mu^2 J^2 \cos^2\frac{k}{2} - 16J^2\Delta^2\cos^4\frac{k}{2} - \Delta^4\sin^2 k. \tag{16}$$

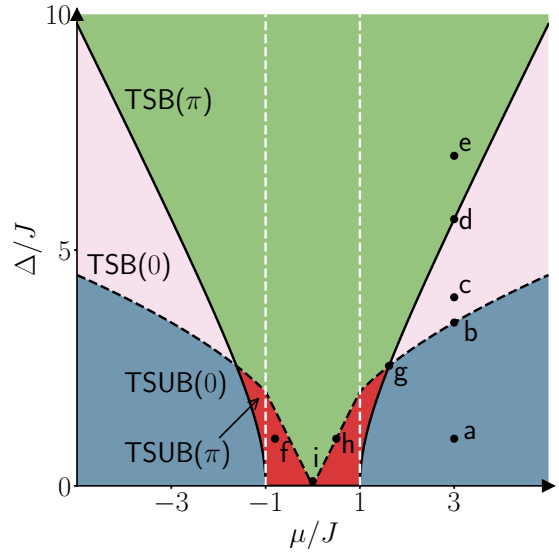

FIG. 2. Phase diagram for a closed chain in μ-Δ parameter plane. The black solid curves indicate the phase boundary, which also separates topological phases identified by the pair Zak phase defined in Eq. (38). Phase boundary is identified by zero-energy gap in Eq. (29). In the nontrivial regions, the Kramer-type degeneracy exists. The reality of the spectrum is differentiated by the black dashed curves, whose form is provided in Eq. (17). It is also the boundary between the $\mathcal{T}$-symmetry-broken and -unbroken regions. (a)–(h) Denote several typical points in different regions and boundaries, which will be investigated in Fig. 3. The phase boundary of the traditional Kitaev chain is indicated by the white dashed lines.

It can been shown that $\mathcal{T}\overline{A}^k_{\rho\sigma}A^k_{\rho\sigma}\mathcal{T}^{-1} = \overline{A}^k_{\rho\sigma}A^k_{\rho\sigma}$ if $\varepsilon^k_{\rho\sigma}$ is real, while $\mathcal{T}\overline{A}^k_{\rho\sigma}A^k_{\rho\sigma}\mathcal{T}^{-1} = \overline{A}^k_{\rho\bar{\sigma}}A^k_{\rho\bar{\sigma}} \neq \overline{A}^k_{\rho\sigma}A^k_{\rho\sigma}$ (with $\bar{\sigma} = -\sigma$ and $\bar{\rho} = -\rho$) when $\varepsilon^k_{\rho\sigma}$ becomes complex, which indicate the symmetry-unbroken and -broken regions. The boundary of two regions in the Δ-μ plane (in unit of J) is

$$\Delta = \begin{cases} 2\mu, & |\mu| < J \\ 2\sqrt{|\mu|J} & |\mu| > J \end{cases} \tag{17}$$

which is plotted in Fig. 2 by the black dashed curves.

However, when we consider a pair of Bogoliubov modes, we find that $\mathcal{T}\overline{A}^k_{\rho\bar{\sigma}}\overline{A}^k_{\rho\sigma}A^k_{\rho\bar{\sigma}}A^k_{\rho\sigma}\mathcal{T}^{-1} = \overline{A}^k_{\rho\bar{\sigma}}\overline{A}^k_{\rho\sigma}A^k_{\rho\bar{\sigma}}A^k_{\rho\sigma}$ is always true. Accordingly, the pair energy

$$E^k_\rho = \varepsilon^k_{\rho+} + \varepsilon^k_{\rho-} = \rho\sqrt{\Lambda_k + r_k}, \tag{18}$$

referred to as pair spectrum, is always real with

$$r_k = \sqrt{x_k^2 + y_k^2}, \tag{19}$$

$$x_k = (2J^2 + \Delta^2)\cos k + 2J^2 - 4\mu^2, \tag{20}$$

$$y_k = \Delta\sqrt{\Delta^2 + 4J^2}\sin k. \tag{21}$$

The expression $r_k(x_k, y_k)$ is crucial for the discussion about topological phase in the following sections.

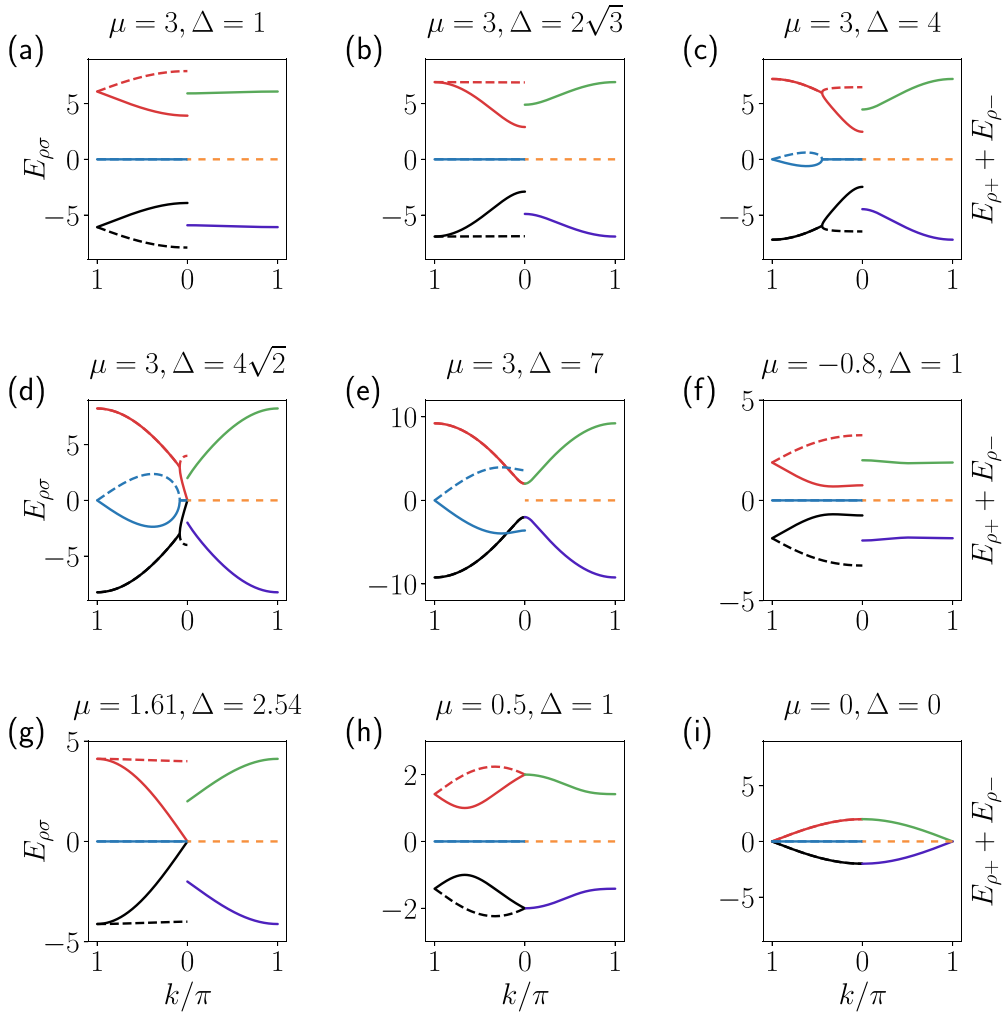

FIG. 3. Energy spectra from Eqs. (14) and (18) for the Hamiltonians at typical points in different regions of Fig. 2. The red dashed (solid) line stands for $\mathrm{Re}(\varepsilon^k_{++})$ [$\mathrm{Re}(\varepsilon^k_{+-})$], and the black dashed (solid) line stands for $\mathrm{Re}(\varepsilon^k_{-+})$ [$\mathrm{Re}(\varepsilon^k_{--})$]. The blue dashed (solid) line stands for $\mathrm{Im}(\varepsilon^k_{--})$ [$\mathrm{Im}(\varepsilon^k_{-+})$]. Similarly, the green (purple) line stands for $\mathrm{Re}(\varepsilon^k_{++} + \varepsilon^k_{+-})/2$ [$\mathrm{Re}(\varepsilon^k_{-+} + \varepsilon^k_{--})/2$], and the orange line stands for $\mathrm{Im}(\varepsilon^k_{--} + \varepsilon^k_{-+})/2$. Other parameter $N = 1000$.

Then, any N_l-quasiparticle eigenstate of the Hamiltonian H can be written in the form

$$\prod_{l=1}^{N_l} \overline{A}^{k_l}_{\rho_l\sigma_l} |\mathrm{Vac}\rangle, \tag{22}$$

with eigenenergy $\sum_{l=1}^{N_l} \varepsilon^{k_l}_{\rho_l\sigma_l}$, which associates with the biorthogonal eigenstate

$$\langle\overline{\mathrm{Vac}}| \prod_{l=1}^{N_l} A^{k_l}_{\rho_l\sigma_l} \tag{23}$$

of the Hamiltonian $H^\dagger$ with eigenenergy $\sum_{l=1}^{N_l} (\varepsilon^{k_l}_{\rho_l\sigma_l})^*$, where $|\mathrm{Vac}\rangle$ ($\langle\overline{\mathrm{Vac}}|$) is the vacuum state of operator $A^{k_l}_{\rho_l\sigma_l}$ ($\overline{A}^{k_l}_{\rho_l\sigma_l}$), defined as $A^{k_l}_{\rho_l\sigma_l}|\mathrm{Vac}\rangle = 0$ ($\langle\overline{\mathrm{Vac}}|\overline{A}^{k_l}_{\rho_l\sigma_l} = 0$). The many-particle eigenstate can have complex eigenenrgy in the broken region. Nevertheless, there is a set of eigenstates which are constructed by a set of pair operators $\{\overline{A}^k_{\rho+}\overline{A}^k_{\rho-}\}$, always possessing real eigenenergy in both broken and unbroken regions. We refer the set of states as BCS-pair states since they contain the pair states $\alpha^\dagger_k\alpha^\dagger_{-k}|0\rangle$, $\beta^\dagger_k\beta^\dagger_{-k}|0\rangle$, $\alpha^\dagger_k\beta^\dagger_{-k}|0\rangle$, and $\alpha^\dagger_{-k}\beta^\dagger_k|0\rangle$, where $|0\rangle$ is the vacuum state of fermion operator c_j. Among them, the one with lowest eigenenergy

$$E_\mathrm{g} = \sum_{k>0} E^k_- \tag{24}$$

is defined as pair ground state

$$|\mathrm{G}\rangle = \prod_{k>0} \overline{A}^k_{\rho+}\overline{A}^k_{\rho-}|\mathrm{Vac}\rangle. \tag{25}$$

In parallel, we have $\langle\overline{\mathrm{G}}| = \langle\overline{\mathrm{Vac}}| \prod_{k>0} A^k_{\rho-}A^k_{\rho+}$ with $\langle\overline{\mathrm{G}}|\mathrm{G}\rangle = 1$, satisfying $\langle\overline{\mathrm{G}}|H = \langle\overline{\mathrm{G}}|E_\mathrm{g}$.

In Fig. 3, we plot the energy spectra for the Hamiltonian at typical points in Fig. 2. The dispersion relation of the quasiparticle obtained in Eq. (14) is plotted on the left side and the pair energy is plotted at the right side. The energy gap closes at the condition $\varepsilon^k_{-+} = \varepsilon^k_{+-}$. The solution is

$$\Delta^2 + 4J^2 - 4\mu^2 = 0. \tag{26}$$

TABLE I. Classification of four quantum phases by the pair Zak phase $\mathcal{Z}$ of the ground state, symmetry of eigenvector, reality of two kinds of spectrum, energy gap, and the edge mode of Majorana lattice.

	TSB(π)	TSUB(π)	TSB(0)	TSUB(0)
Eigenvector symmetry	no	yes	no	yes
Eigenspectrum	complex	real	complex	real
Pair spectrum	real	real	real	real
Pair-spectrum gap	yes	yes	yes	yes
Edge mode	yes	yes	no	no
Typical point	e	f	c	a

In the following several sections, we will prove that the system experiences topological phase transition when the closing occurs, which is the main focus of our investigation. The boundary is plotted in Fig. 2 by the black solid curves. It shows that the phase diagram is extended in μ direction as Δ increases comparing to that of traditional Kitaev chain indicated by the white dashed lines. Now, with the help of Eqs. (17) and (26), the phase diagram can be distinguished into four parts. We classified these four regions by the pair Zak phase $\mathcal{Z}$ of the ground state, which will be introduced in detail in Sec. IV, and the time-reversal symmetry of the eigenvectors. They are listed as follows: (i) time symmetry is broken with $\mathcal{Z}=\pi$ [TSB(π)]; (ii) time symmetry is unbroken with $\mathcal{Z}=\pi$ [TSUB(π)]; (iii) time symmetry is broken with $\mathcal{Z}=0$ [TSB(0)]; (iv) time symmetry is unbroken with $\mathcal{Z}=0$ [TSUB(0)].

The spectrum properties of the four phases are summarized in Table I, which clearly indicates the distinction between two phases. In Fig. 2, we mark the different phases with different colors. Figure 3 reveals these properties straightforwardly. (i) At the phase boundary, (d) and (g), positive and negative branches touch at $k=0$. Otherwise there are energy gap. (ii) In TSUB regions, (a) and (f), four branches are all real. In TSB regions, (c), (d), and (e), all of them become complex. (iii) At the $\mathcal{T}$-symmetry-broken boundary, (b), (g), and (h), the branches are still real. A slight increase of Δ or decrease of μ can result in the appearance of complex energy levels from $k=\pi$. For the point (i), the model reduces to a noninteracting Hermitian model. Notably, we note that all curves of $(\varepsilon^k_{\rho+}+\varepsilon^k_{\rho-})/2$ are real. In addition, the classification of phases is independent of the boundary conditions. In fact, it can also be obtained from an open chain since (i) the spectrum of a system is independent of the boundary conditions large N, and (ii) the Zak phase for a ring system is equivalent to the number of zero modes of Majorana lattice with open boundary condition, according to the bulk-boundary correspondence. In the following, we will investigate the phase diagram based on the properties of the pair ground state ($|\mathrm{G}\rangle$, $\langle\overline{\mathrm{G}}|$).

III. PHASE DIAGRAM AND ORDER PARAMETER

In general, a quantum phase transition for a Hermitian system occurs when the ground state experiences sudden change [17]. The phase boundary in parameter space is characterized by the opening or closing of the energy gap between ground and first excited states. Remarkably, it is always associated with discontinuity of the derivative of density of ground-state energy, or other observables, and even the change of topological index for topological quantum phase transition. It is worthy to investigate the present system systematically due to its non-Hermiticity. Two main questions should be addressed: (i) Is there a conventional quantum phase transition for the pair ground state of such a non-Hermitian system? (ii) What happens in the pair ground state at symmetric broken boundary?

According to the theory of quantum phase transition in a Hermitian system, the quantum phase boundary locates at the degenerate point, or gap-closing point. For the present system, it corresponds to $\varepsilon^{k_c}_{\rho-}=0$, which determines the phase boundary in the parameter space. From equation $\varepsilon^{k_c}_{\rho-}=0$, we have $r_{k_c}=\sqrt{x^2_{k_c}+y^2_{k_c}}=0$, or explicitly

$$\left(2J_c^2+\Delta_c^2\right)\cos k_c+2J_c^2-4\mu_c^2=0, \tag{27}$$

$$\sqrt{\Delta_c^4+4\Delta_c^2J_c^2}\sin k_c=0. \tag{28}$$

The solution is $k_c=0$, resulting in the phase boundary

$$\Delta_c^2+4J_c^2-4\mu_c^2=0, \tag{29}$$

which is plotted in Fig. 2 by the black solid curves. We note that the quantum phase transition occurs at the zero point of $r_k=\sqrt{x_k^2+y_k^2}$, which is crucial for the investigation of topological quantum phase transition in the next section. When taking $\Delta_c=0$, the phase boundary reduces to $\mu_c=\pm J_c$ (white dashed lines in Fig. 2), which is the one for the standard Hermitian Kitaev chain. In this regard, the present phase diagram is extended in μ direction as Δ increases comparing to that of traditional Kitaev chain.

Now we consider the behavior of the density of ground-state energy ε_{g}. In thermodynamic limit $N\to\infty$, we have

$$\varepsilon_{\mathrm{g}}=\frac{E_{\mathrm{g}}}{2N}=\frac{1}{2\pi}\int_0^{\pi}E^k_-dk. \tag{30}$$

We note that the integrand E^k_- at $k=0^+$

$$E^{0^+}_-=-\sqrt{4\mu^2+4J^2-\Delta^2+|x_{0^+}|} \tag{31}$$

contains a term

$$|x_{0^+}|=\left|\Delta^2+4J^2-4\mu^2\right|, \tag{32}$$

which is nonanalytic at the boundary, i.e., $|x_{0^+}|=0$, resulting nonanalytic ε_{g}. Accordingly, it indicates the discontinuity of $(\partial\varepsilon_{\mathrm{g}}/\partial\Delta,\partial\varepsilon_{\mathrm{g}}/\partial\mu)$ and divergence of $(\partial^2\varepsilon_{\mathrm{g}}/\partial\Delta^2,\partial^2\varepsilon_{\mathrm{g}}/\partial\mu^2)$, or the occurrence of second-order quantum phase transition.

Now, we introduce two kinds of parameters that can identify quantum phase transitional behavior. They are the analog of pair order parameter in a Hermitian superconducting system $\langle F\rangle$ and the average of particle density $\langle n\rangle$. Based on the non-Hermitian version of Hellmann-Feynman theorem [35] and the translational symmetry of the ground state, we have the relations

$$\langle F\rangle=\frac{1}{2}\langle\overline{\mathrm{G}}|(c^\dagger_{2j+1}c^\dagger_{2j}+c_{2j-1}c_{2j})|\mathrm{G}\rangle=\frac{\partial\varepsilon_{\mathrm{g}}}{\partial\Delta} \tag{33}$$

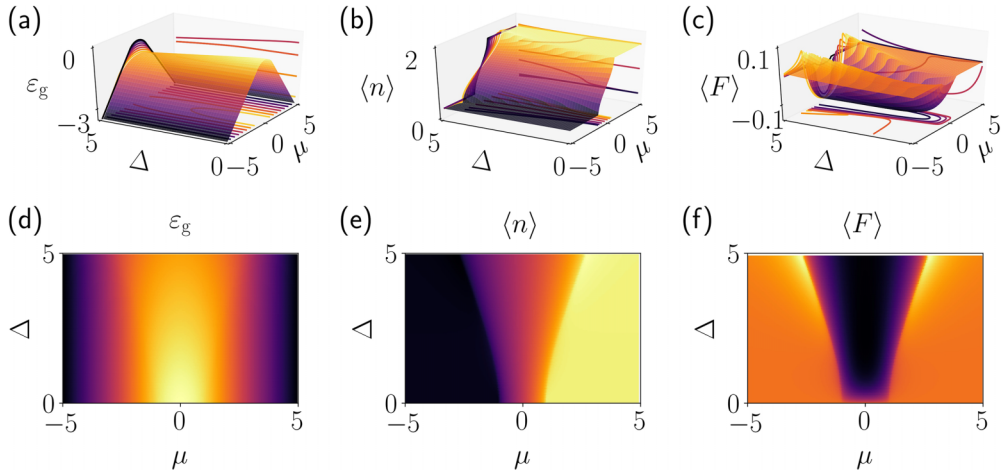

FIG. 4. 3D plots of (a) ε_g, (b) $\langle n\rangle$, and (c) $\langle F\rangle$ obtained from Eqs. (30), (34), and (33), respectively. (d)–(f) The corresponding top views of them. It can be seen that $\langle n\rangle$ and $\langle F\rangle$ are discontinuous at the phase boundary. Other parameter is $N = 4000$.

and

$$\langle n\rangle = \langle \overline{\mathrm{G}}|n_l|\mathrm{G}\rangle = 1 - \frac{\partial \varepsilon_g}{\partial \mu}, \tag{34}$$

with $l \in [1, 2N]$ and $j \in [1, N]$, where $\langle \dots \rangle$ denotes the expectation value for the ground state in the framework of biorthogonal inner product. The choice of biorthogonal inner product guarantees the restriction $\langle n\rangle \leqslant 1$, in comparison with the Dirac inner product.

It is clear that quantities $\langle F\rangle$ and $\langle n\rangle$ are discontinuous at the boundary. It is natural to ask what happens at quantum phase transition boundary? To answer the question, numerical simulation is performed for the finite system. $\langle F\rangle$ and $\langle n\rangle$ as functions of (Δ, μ) are plotted in Fig. 4, which indicates that two quantities can be served as order parameters for characterizing the quantum phase transitions only when they experience a jump at the quantum phase boundary.

We note that the phase boundary in Eq. (29) is Δ dependent, while the white dashed lines in Fig. 2 are Δ independent. In order to understand such a difference, we consider a Hermitian Kitaev model with Hamiltonian $\mathcal{H} = H + H^\dagger$. The reason can be understood from the following analysis. Based on the Fourier transformation, we have

$$H = H_{k=0} + \sum_{k\in(0,\pi]} H_k, \tag{35}$$

where

$$\begin{aligned} H_{k=0} &= 2J\beta_0^\dagger\alpha_0 + \mathrm{H.c.} + \Delta\beta_0\alpha_0 \\ &\quad + \Delta\beta_0^\dagger\alpha_0^\dagger + \mu(2 - 2\beta_0^\dagger\beta_0 - 2\alpha_0^\dagger\alpha_0). \end{aligned} \tag{36}$$

This term is neglected in the above as usual for the sake of simplicity since the role of $H_{k=0}$ can be obtained from the limit $k \to 0$. The boundary for H can be determined by $H_{k=0}$ since the eigenenergy $\varepsilon_{k=0} = \sqrt{4\mu^2 - \Delta^2} - 2J$, which is the minimum of the excitations. From $\varepsilon_{k=0} = 0$ we then have $\Delta_c^2 + 4J_c^2 - 4\mu_c^2 = 0$. However, for $\mathcal{H}$ the pair term in $H_{k=0} + H_{k=0}^\dagger$ is canceled, which results in the conclusion that the boundary for $\mathcal{H}$ is independent of Δ. In this sense, the stability of the boundary for $\mathcal{H}$ comes from the balance (or cancellation) of pair terms in H and $H^\dagger$, respectively.

IV. TOPOLOGICAL PHASE

In this section, we investigate the quantum phase from perspective of topology. It is well known that the superconducting phase in the Hermitian model is topologically nontrivial, which is characterized by winding number and demonstrated by edge modes in Majorana lattice [12]. In this section, we investigate this issue for the present model. As mentioned above, the pair dispersion contains the term $r_k = \sqrt{x_k^2 + y_k^2}$, which has a zero point when the system locates at the phase boundary. The previous work [36] implies that there is a hidden ellipse with parameter equation (x_k, y_k) in the ground state. Next, we will extract the topological index from the wave function of the pair ground state. To characterize the property of the energy band, we give the expression of Zak phase

$$z_{\rho\sigma} = i\int_0^{2\pi} \langle \overline{\mathrm{Vac}}|A_{\rho\sigma}^k \frac{\partial}{\partial k}\overline{A}_{\rho\sigma}^k|\mathrm{Vac}\rangle dk. \tag{37}$$

$z_{\rho\sigma}$ is not an integer over π in general case. In this work, to characterize the property of the ground state, we study the Zak phase of the lowest-energy band of the pair spectrum. Our strategy is to calculate the Berry flux of pair state $|\Psi_k\rangle = \overline{A}_{-+}^k\overline{A}_{--}^k|\mathrm{Vac}\rangle$

$$\mathcal{Z} = i\int_0^{2\pi} \mathcal{A}_k dk, \tag{38}$$

where the Berry connection is given by

$$\mathcal{A}_k = \langle \overline{\Psi_k}| \frac{\partial}{\partial k}|\Psi_k\rangle, \tag{39}$$

with $\langle\overline{\Psi_k}| = \langle\overline{\mathrm{Vac}}|A_{--}^k A_{-+}^k$. Notably, pair Zak phase $\mathcal{Z}$ can also be obtained via

$$\mathcal{Z} = z_{-+} + z_{--}. \tag{40}$$

In Fig. 5(c), the total Zak phase is numerically demonstrated in parameter space. The solid black line $\Delta = 2\sqrt{\mu^2 - J^2}$ indicates the boundary between the trivial and nontrivial topological phase regions. It can be easily found that this line is also the phase boundary in Fig. 2. As a

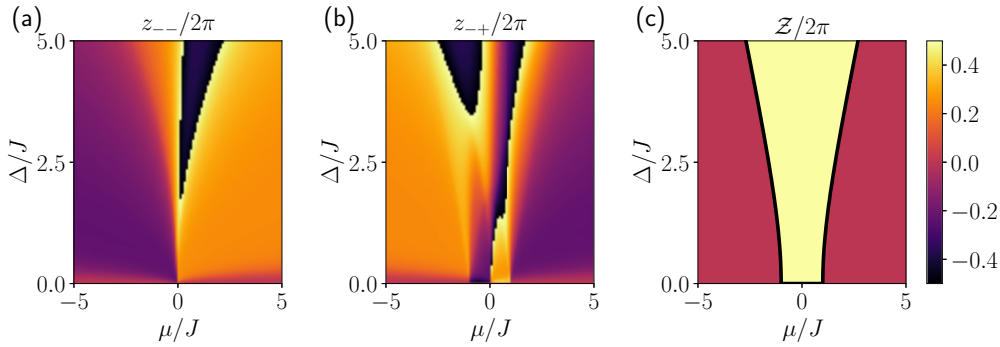

FIG. 5. 2D contour color plots of (a) z_{--}, (b) z_{-+}, and (c) $\mathcal{Z}$, as functions of μ and Δ, obtained from numerical results of Eqs. (37) and (38) on $N = 51$ lattice. It can be seen that z_{-+} and z_{--} are both irregular, while $\mathcal{Z}$ is quantized and accords with the phase boundary in (29) indicated by the black solid lines.

comparison, z_{--} and z_{-+} are also plotted in Figs. 5(a) and 5(b), respectively. We notice that the symmetry breaking has no effect on the ground state and $\mathcal{Z}$, which accords with the edge states discussed in the following sections.

V. BULK-BOUNDARY CORRESPONDENCE

Let us now turn to the discussion on bulk-edge correspondence in such a non-Hermitian system to investigate the influence from the non-Hermiticity. Based on the above analysis, it turns out that the bulk system exhibits the similar topological feature within the symmetry-unbroken regions. In Hermitian systems, the existence of edge modes is intimately related to the bulk topological quantum numbers, which is referred to as the bulk-edge correspondence [37–40]. We are interested in the generalization of the bulk-edge correspondence to non-Hermitian systems. Previous works have shown that when sufficiently weak non-Hermiticity is introduced to topological insulator models, the edge modes can retain some of their original characteristics [41,42]. For a non-Hermitian Hamiltonian with full real spectrum, there is a Hermitian counterpart within the symmetry-unbroken region [2,4,9–11,43–47]. Then, the bulk-edge correspondence can be established based on the Hermitian counterpart [24]. Next, we will show that the topological phase still exists even in the symmetric-broken region for the present Hamiltonian, with the existence of edge modes.

Considering the spinless fermion system with an open boundary condition, the Hamiltonians read as

$$H_{\mathrm{CH}} = H - M, \tag{41}$$

$$M = \Delta c_{2N}^{\dagger} c_1^{\dagger} + J c_{2N}^{\dagger} c_1 + J c_1^{\dagger} c_{2N}. \tag{42}$$

We introduce Majorana fermion operators

$$a_j = c_j^{\dagger} + c_j, \quad b_j = -i(c_j^{\dagger} - c_j), \tag{43}$$

which satisfy the relations

$$\{a_j, a_{j'}\} = 2\delta_{j,j'}, \quad \{b_j, b_{j'}\} = 2\delta_{j,j'}, \tag{44}$$

$$\{a_j, b_{j'}\} = 0. \tag{45}$$

The inverse transformation is

$$c_j^{\dagger} = \tfrac{1}{2}(a_j + i b_j), \quad c_j = \tfrac{1}{2}(a_j - i b_j). \tag{46}$$

The Majorana representation of the Hamiltonian has the form

$$\begin{aligned} H_{\mathrm{CH}} = \sum_{j=1}^{N} \Big[& i\Big(\frac{J}{4} + \frac{\Delta}{8}\Big)(-a_{2j-1}b_{2j} - a_{2j}b_{2j+1}) \\ & + i\Big(\frac{J}{4} - \frac{\Delta}{8}\Big)(b_{2j-1}a_{2j} + b_{2j}a_{2j+1})\Big] + \mathrm{H.c.} \\ & - \frac{\Delta}{4}(a_{2j}a_{2j-1} + a_{2j}a_{2j+1} + b_{2j+1}b_{2j} + b_{2j-1}b_{2j}) \\ & - \frac{\mu}{2}\sum_{j=1}^{2N}(i b_j a_j + \mathrm{H.c.}). \end{aligned} \tag{47}$$

Based on the identities

$$c_l^{\dagger} c_{l+1} + \mathrm{H.c.} = i b_j a_{j+1} = \frac{1}{2}(b_j, -i a_{j+1}) \begin{pmatrix} 0 & 1 \\ 1 & 0 \end{pmatrix} \begin{pmatrix} b_j \\ i a_{j+1} \end{pmatrix}, \tag{48}$$

$$n_l = i b_j a_j = \frac{1}{2}(-i a_j, b_j) \begin{pmatrix} 0 & 1 \\ 1 & 0 \end{pmatrix} \begin{pmatrix} i a_j \\ b_j \end{pmatrix}, \tag{49}$$

and

$$c_{2j+1}^{\dagger} c_{2j}^{\dagger} = \frac{1}{8}\varphi_1^{\dagger} \begin{pmatrix} 0 & 0 & -1 & 1 \\ 0 & 0 & -1 & 1 \\ 1 & -1 & 0 & 0 \\ 1 & -1 & 0 & 0 \end{pmatrix} \varphi_1, \tag{50}$$

$$c_{2j-1} c_{2j} = \frac{1}{8}\varphi_2^{\dagger} \begin{pmatrix} 0 & 0 & 1 & 1 \\ 0 & 0 & -1 & -1 \\ -1 & -1 & 0 & 0 \\ 1 & 1 & 0 & 0 \end{pmatrix} \varphi_2, \tag{51}$$

where $\varphi_1^{\dagger} = (-i a_{2j}, b_{2j}, -i a_{2j+1}, b_{2j+1})$ and $\varphi_2^{\dagger} = (-i a_{2j-1}, b_{2j-1}, -i a_{2j}, b_{2j})$, we write the Hamiltonian in the basis $\varphi^{\dagger} = (-i a_1, b_1, -i a_2, b_2, -i a_3, b_3, \dots)$ and see that

$$H_{\mathrm{CH}} = \varphi^{\dagger} h_{\mathrm{CH}} \varphi, \tag{52}$$

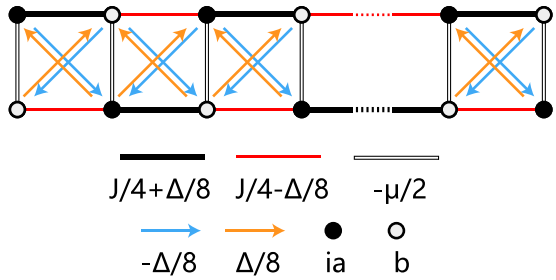

FIG. 6. Geometry for the Majorana lattice described in Eq. (53) with an open boundary. The system consists of two sublattices, *ia* and *b*, indicated by solid and empty circles, respectively. The black solid lines, the red solid lines, and the double lines indicate the couplings between the sublattices. The yellow and blue arrows are the unidirectional hoppings. The eigenmodes near zero eigenvalue are plotted in Fig. 7.

where h_{CH} represents a $4N\times4N$ matrix. Here matrix h_{CH} can be explicitly written as

$$\begin{aligned} h_{\mathrm{CH}} =& \left(\frac{J}{4}+\frac{\Delta}{8}\right)\sum_{j=1}^{N}(|2j-1\rangle_{AB}\langle 2j|+|2j\rangle_{AB}\langle 2j+1|) \\ &+\left(\frac{J}{4}-\frac{\Delta}{8}\right)\sum_{j=1}^{N}(|2j-1\rangle_{BA}\langle 2j|+|2j\rangle_{BA}\langle 2j+1|) \\ &-\frac{\mu}{2}\sum_{j=1}^{2N}|j\rangle_{AB}\langle j|+\mathrm{H.c.} \\ &-\frac{\Delta}{8}\sum_{j=1}^{N}(|2j\rangle_{AA}\langle 2j-1|+|2j\rangle_{AA}\langle 2j+1|-\mathrm{H.c.}) \\ &-\frac{\Delta}{8}\sum_{j=1}^{N}(|2j-1\rangle_{BB}\langle 2j|+|2j+1\rangle_{BB}\langle 2j|-\mathrm{H.c.}), \end{aligned} \tag{53}$$

where basis $\{|l\rangle_A, |l\rangle_B, l\in[1,2N]\}$ is an orthonormal complete set, ${}_A\langle l|l'\rangle_B=\delta_{ll'}\delta_{AB}$, which accords with φ. Schematic illustration for structure of h_{CH} is described in Fig. 6 by different types of nodal lines.

The edge states at the limitation of infinity large size system ($N\longrightarrow\infty$) are analytically obtained. For the case with $\Delta>2\sqrt{\mu^2-J^2}$, the edge states of h_{CH} are in the form of

$$|\psi_{\mathrm{L}}\rangle=\frac{1}{\sqrt{\Omega}}\sum_{j=1}^{2N}[(\gamma_1)^j-(\gamma_2)^j]|\widetilde{j_1}\rangle, \tag{54}$$

$$|\psi_{\mathrm{R}}\rangle=\frac{1}{\sqrt{\Omega}}\sum_{j=1}^{2N}[(\gamma_1)^{2N+1-j}-(\gamma_2)^{2N+1-j}]|\widetilde{j_2}\rangle, \tag{55}$$

where the kets are

$$|\widetilde{j_1}\rangle=|j\rangle_A+(-1)^j\beta|j\rangle_B, \tag{56}$$

$$|\widetilde{j_2}\rangle=|j\rangle_B+(-1)^{2N+1-j}\beta|j\rangle_A \tag{57}$$

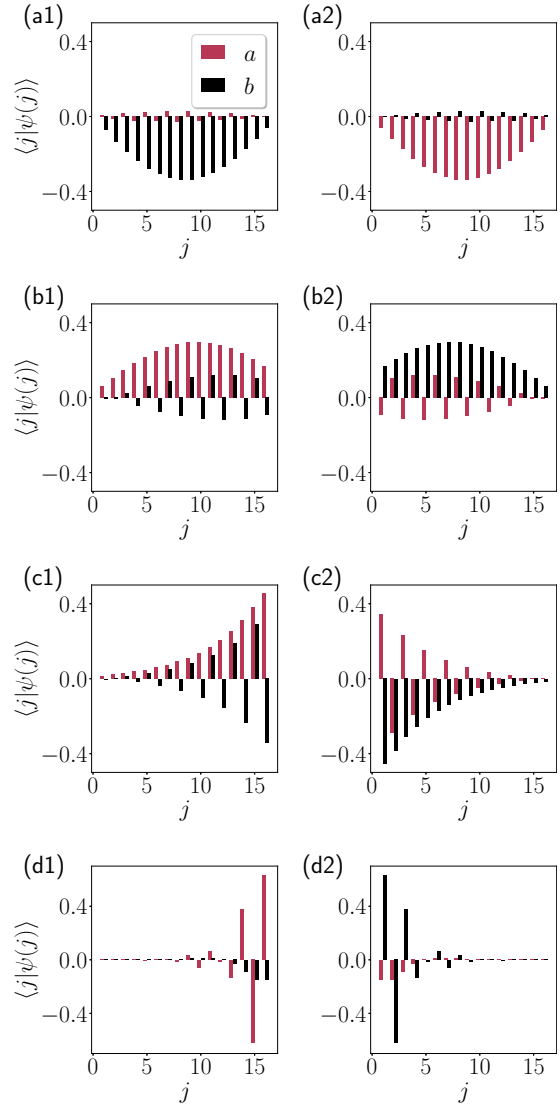

FIG. 7. The amplitude distribution of eigenmodes of the Majorana lattices in Fig. 6 near the zero eigenvalue obtained from exact diagonalization on $N=8$ lattice at four different colored regions in Fig. 2. (a) $\mu=3$, $\Delta=1$, in blue region; (b) $\mu=3$, $\Delta=4$, in pink region; (c) $\mu=3$, $\Delta=7$, in green region; and (d)$\mu=-0.8$, $\Delta=1$, in red region. The color bar indicates the amplitude of wave function. The profile of edge modes accords with the the expression in Eqs. (54) and (55). It is shown that existence of nonzero quantized Zak phase always associated with edge modes, demonstrating the bulk-edge correspondence.

with the coefficients

$$\gamma_l=\frac{2\mu+(-1)^l2\sqrt{\mu^2-J^2}}{\sqrt{\Delta^2+4J^2}+\Delta} \tag{58}$$

and

$$\beta=\sqrt{1+(2J/\Delta)^2}+2J/\Delta, \tag{59}$$

and Ω is the normalization factor. The derivations of the analysis form of the edge states are presented in Appendix A 2. We plot the distribution of particle amplitude $p(j)$ of $|\psi_{\mathrm{L}}\rangle$ and $|\psi_{\mathrm{R}}\rangle$ in Fig. 7. In contrast, there is no zero mode for

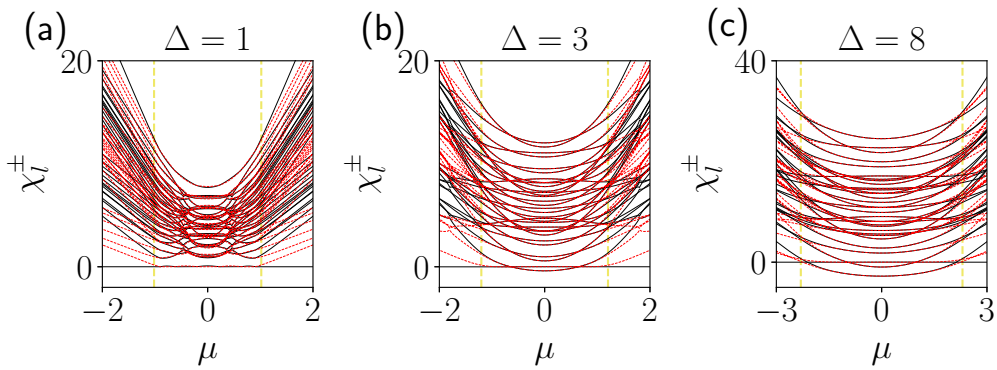

FIG. 8. The plot of $\chi_l^{\pm}$ as a function of μ, obtained through exact diagonalization. System parameters: $N = 6$ and $J = 1$. Red dashed lines represent the values of $\{\chi_l^{+}\}$ and the black lines represent the values of $\{\chi_l^{-}\}$. Notably, all energy levels become twofold degeneracy simultaneously at one point which is marked by the yellow dashed lines, protected by the symmetry of the operators $\overline{D}, D$. The degeneracy point gradually approaches the topological nontrivial boundary as N increases.

$\Delta < 2\sqrt{\mu^2 - J^2}$, which indicates the coexistence of zero modes and nonzero Zak phases, demonstrating the bulk-edge correspondence.

VI. KRAMER-TYPE DEGENERACY

In this section, we further elucidate the implication of the Majorana zero modes on the feature of the system and how it provides an evident signature of the phase diagram regardless of the appearance of the complex energy levels.

The parity and time-reversal symmetries of H always hold for finite-size ring or chain. Inspired from the previous works [48,49], the present Hamiltonian in thermodynamic limit also possesses a conditional symmetry in the topological phase, although it is non-Hermitian system. It is due to the existence of zero modes in the Majorana lattice. Based on the exact expression of $|\psi_{\mathrm{L,R}}\rangle$ and $\overline{|\psi_{\mathrm{L,R}}\rangle}$, one can construct a set of nonlocal operators

$$D = \frac{i}{2\sqrt{\Omega}} \sum_{j=1}^{2N} [(\gamma_1)^j - (\gamma_2)^j][(-1)^j \beta d_1^{\dagger} + d_2], \quad (60)$$

$$\overline{D} = \frac{i}{2\sqrt{\Omega}} \sum_{j=1}^{2N} [(\gamma_1)^j - (\gamma_2)^j][(-1)^j \beta d_1 - d_2^{\dagger}], \quad (61)$$

with

$$d_1 = c_{2N+1-j}^{\dagger} - c_j^{\dagger} + c_{2N+1-j} + c_j, \quad (62)$$

$$d_2 = c_{2N+1-j} - c_j - c_{2N+1-j}^{\dagger} - c_j^{\dagger}, \quad (63)$$

which satisfy the commutation relations

$$[D, H_{\mathrm{CH}}] = [\overline{D}, H_{\mathrm{CH}}] = 0 \quad (64)$$

and

$$\{D, \overline{D}\} = 1, \ \overline{D}^2 = D^2 = 0. \quad (65)$$

Considering the set of complete eigenstates $\{|\psi_n^{+}\rangle, |\psi_n^{-}\rangle\}$ of H with eigenenergy $\varepsilon_n^{\pm}$, $H|\psi_n^{\pm}\rangle = \varepsilon_n^{\pm}|\psi_n^{\pm}\rangle$, where

$$\Pi|\psi_n^{\pm}\rangle = \pm|\psi_n^{\pm}\rangle, \quad (66)$$

we have the relations

$$D|\psi_n^{+}\rangle = |\psi_n^{-}\rangle, \quad \overline{D}|\psi_n^{-}\rangle = |\psi_n^{+}\rangle, \quad (67)$$

$$\overline{D}|\psi_n^{+}\rangle = D|\psi_n^{-}\rangle = 0, \quad (68)$$

which guarantee the existence of eigenstate degeneracy $\varepsilon_n^{+} = \varepsilon_n^{-} = \varepsilon_n$, referred to as Kramer-type degeneracy [48,49]. Note that here ε_n can be complex energy.

Let us now examine the performance of our finding in finite-size system. To demonstrate this point, numerical results are presented. The spectrum of Kitaev Hamiltonian H_{CH} on finite chain can be obtained numerically. We reorder the complex energy level $\{\varepsilon_n^{\pm}\}$ by the value of $\mathcal{E}_l^{\pm} = \mathrm{Re}\ \varepsilon_n^{\pm} + \mathrm{Im}\ \varepsilon_n^{\pm}$, and calculate the mode of the relative value

$$\chi_l^{\pm} = |\mathcal{E}_l^{\pm} - \mathcal{E}_1|, \quad (69)$$

where $\mathcal{E}_1$ means the smallest value in $\{\mathcal{E}_n^{\pm}\}$. Figures 8(a)–8(c) plot $\chi_l^{\pm}(\mu, \Delta)$ for $\Delta = J$, $3J$, and $8J$, as functions of μ. As expected, the complete spectrum $\chi_l^{\pm}$ becomes twofold degeneracy approximately within the nontrivial regions. The μ-parameter regime of degeneracy that been illustrated by yellow dashed lines in Fig. 8 widens with Δ.

VII. SUMMARY

In summary, we have analyzed a one-dimensional non-Hermitian Kitaev model with locally imbalanced but globally balanced pair creation and annihilation, which is introduced by staggered non-Hermitian pairing terms. It exhibits the similar topological features compared with the original Hermitian one, but modifies the phase boundary. In parallel, a nontrivial topological phase is always associated with edge states in the open chain, in which the Zak phase is defined in the terms of biorthonormal inner product for the BCS-type pair wave function. Correspondingly, the edge modes are obtained with the aid of the Majorana transformation, resulting in the Kramer-type degeneracy of both the real and complex levels as a signature of the topologically nontrivial phase. These results indicate that the staggered non-Hermitian pairing terms still

create superconducting phases and their topological feature is immune to the non-Hermitian effect. This study provides the insight into the topological phase emerged from the interplay between spatially separated pairing processes. Experimentally, the Majorana can be realized in photonic system and the edge modes can be detected [50]. Recently, it has been shown that the phase diagram of a Hermitian Kitaev model can be demonstrated in the dynamic process [51]. This will be an interesting topic for our future work to investigate the dynamics of the present model.

ACKNOWLEDGMENT

We acknowledge the support of the National Natural Science Foundation of China (Grant No. 11874225).

APPENDIX: DERIVATIONS OF BOGOLIUBOV MODES AND EDGE MODES

In this Appendix, the derivations of Bogoliubov modes in Eq. (14) and edge modes in Eqs. (54) and (55) are presented.

1. Bogoliubov modes

Consider the matrix

$$h_k = \begin{pmatrix} -2\mu & \gamma_k & 0 & -\Delta_o e^{ik} \\ \gamma_k^* & -2\mu & \Delta_o e^{-ik} & 0 \\ 0 & -\Delta_e & 2\mu & -\gamma_k \\ \Delta_e & 0 & -\gamma_k^* & 2\mu \end{pmatrix}, \tag{A1}$$

which can be written as the form

$$h_k = \begin{pmatrix} -a & b & 0 & -c \\ b^* & -2\mu & c^* & 0 \\ 0 & -d & 2\mu & -b_k \\ d & 0 & -b_k^* & a \end{pmatrix}, \tag{A2}$$

by the substitutions

$$a = 2\mu,\ b = \gamma_k,\ c = \Delta_o e^{ik},\ d = \Delta_e. \tag{A3}$$

Here we remain using the parameters Δ_o and Δ_e rather than Δ. We will show that the solution only depends on $\Delta_o\Delta_e$. Taking a similarity transformation the matrix h_k is diagonalized as

$$V^k h_k \overline{V}^k = \begin{pmatrix} \varepsilon_{++}^k & 0 & 0 & 0 \\ 0 & \varepsilon_{+-}^k & 0 & 0 \\ 0 & 0 & \varepsilon_{--}^k & 0 \\ 0 & 0 & 0 & \varepsilon_{-+}^k \end{pmatrix}, \tag{A4}$$

where the eigenvalue is

$$\varepsilon_{\rho\sigma}^k = \rho\sqrt{\Lambda_k + \sigma\sqrt{\Omega_k}}, \tag{A5}$$

with $\rho, \sigma = \pm$ and $\overline{V}^k = (V^k)^{-1}$. Here the parameters are

$$\begin{aligned} \Lambda_k &= a^2 + |b|^2 - \frac{(cd + c^*d)}{2} \\ &= 4\mu^2 - \Delta_o\Delta_e \cos k + 4J^2 \cos^2 \frac{k}{2} \end{aligned} \tag{A6}$$

and

$$\begin{aligned} \Omega_k &= -cd(b^*)^2 + 4a^2|b|^2 - cd|b|^2 - dc^*|b|^2 \\ &\quad - c^*db^2 - \frac{d^2|c|^2}{2} + \frac{c^2d^2 + c^{*2}d^2}{4} \\ &= 64\mu^2J^2 \cos^2 \frac{k}{2} - (\Delta_o\Delta_e)^2 \sin^2 k \\ &\quad - 16J^2\Delta_o\Delta_e \cos^4 \frac{k}{2}, \end{aligned} \tag{A7}$$

which only depends on $\Delta_o\Delta_e$, and then can be replaced by $\Delta = \sqrt{\Delta_o\Delta_e}$ for positive Δ_o and Δ_e. The explicit form of V^k and $\overline{V}^k$ can be obtained from the eigenvector $\Psi_{\rho\sigma}$ of eigenvalue $\varepsilon_{\rho\sigma}^k$:

$$\Psi_{\rho\sigma} = \begin{pmatrix} 8a|b|^2 + 2(dc^* - cd + 2\rho\sqrt{\Omega_k})(a - \varepsilon_{\rho\sigma}) \\ 2[2bdc^* + b^*(cd + dc^* - 4a^2 - 2\rho\sqrt{\Omega_k} + 4a\varepsilon_{\rho\sigma})] \\ 4d[ab - ab^* + (b + b^*)\varepsilon_{\rho\sigma}] \\ 2d[cd - 2|b|^2 - 2(b^*)^2 - dc^* - 2\rho\sqrt{\Omega_k}] \end{pmatrix} \tag{A8}$$

or

$$\begin{pmatrix} 64\mu J^2 \cos^2 \frac{k}{2} + (4\mu - 2\varepsilon_{\rho\sigma})(\rho\sqrt{\Omega_k} - i2\Delta^2 \sin k) \\ 2J\gamma_k\left(-16\mu^2 - \rho\sqrt{\Omega_k} + 8\mu\varepsilon_{\rho\sigma} + 8\Delta^2 \cos^2 \frac{k}{2}\right) \\ 16\Delta J(\varepsilon_{\rho\sigma} \cos^2 \frac{k}{2} + i\mu \sin k) \\ 2\Delta(-\rho\sqrt{\Omega_k} - 8J^2\gamma_k \cos^2 \frac{k}{2} + i2\Delta^2 \sin k) \end{pmatrix}. \tag{A9}$$

2. The derivations of the edge states

The Bethe ansatz wave function of the edge mode localized at left side $|\psi_L\rangle$ for the matrix h_{CH} has the form

$$\begin{aligned} |\psi_L\rangle = \frac{1}{\sqrt{\Omega}} \sum_{j=1}^{2N} \sum_{l=1,2} \alpha_l(\gamma_l)^{2j}(|2j-1\rangle_A \\ + \beta|2j-1\rangle_B + \gamma_l|2j\rangle_A - \beta\gamma_l|2j\rangle_B), \end{aligned} \tag{A10}$$

where Ω is the normalization factor. The Schrődinger equation

$$h_{CH}|\psi_L\rangle = 0 \tag{A11}$$

gives that γ_1 and γ_2 satisfy the same equations

$$\frac{4\mu\gamma_l}{1 + (\gamma_l)^2} = \Delta\left[\frac{1 - (\gamma_l)^2}{1 + (\gamma_l)^2} + \beta\right] + 2J, \tag{A12}$$

$$\frac{4\mu\gamma_l}{1 + (\gamma_l)^2} = \Delta\left[\frac{1 - (\gamma_l)^2}{1 + (\gamma_l)^2} + \frac{1}{\beta}\right] - 2J. \tag{A13}$$

After a straightforward algebra, we have the nontrivial solutions

$$\gamma_l = \frac{2\mu + (-1)^l 2\sqrt{\mu^2 - J^2}}{\sqrt{\Delta^2 + 4J^2} + \Delta} \tag{A14}$$

and

$$\beta = \sqrt{1 + (2J/\Delta)^2} + 2J/\Delta. \tag{A15}$$

The ratio of α_1 and α_2 is

$$\alpha_1\gamma_1 + \alpha_2\gamma_2 = 0, \tag{A16}$$

obtained by the boundary condition at $j = 1$. Similarly, the wave function of the edge mode localized at right side $|\psi_R\rangle$ can also be obtained. In summary, we have

$$|\psi_L\rangle = \frac{1}{\sqrt{\Omega}} \sum_{j=1}^{2N} [(\gamma_1)^j - (\gamma_2)^j] \widetilde{|j_1\rangle}, \tag{A17}$$

$$|\psi_R\rangle = \frac{1}{\sqrt{\Omega}} \sum_{j=1}^{2N} [(\gamma_1)^{2N+1-j} - (\gamma_2)^{2N+1-j}] \widetilde{|j_2\rangle}, \tag{A18}$$

where the kets

$$\widetilde{|j_1\rangle} = |j\rangle_A + (-1)^j \beta |j\rangle_B, \tag{A19}$$

$$\widetilde{|j_2\rangle} = |j\rangle_B + (-1)^{2N+1-j} \beta |j\rangle_A. \tag{A20}$$

Two states $|\psi_L\rangle$ and $|\psi_R\rangle$ are localized states in the nontrivial regions due to the following facts. (i) In the case with $J < |\mu| < \sqrt{\Delta^2/4 + J^2}$, γ_1 and γ_2 are real and it is easy to check that $|\gamma_1| < 1$ and $|\gamma_2| < 1$. (ii) In the case with $|\mu| < J$, γ_1 and γ_2 become complex number and have the form

$$\gamma_1 = (\gamma_2)^* \tag{A21}$$

with

$$|\gamma_1| = |\gamma_2| = \frac{2J}{\sqrt{\Delta^2 + 4J^2} + \Delta} < 1 \tag{A22}$$

and

$$\arg \gamma_2 = -\arg \gamma_1 = \tan^{-1} \frac{\sqrt{\mu^2 - J^2}}{\mu}. \tag{A23}$$

It can be checked that

$$(\gamma_1)^j - (\gamma_2)^j = i2|\gamma_1|^j \sin(j \arg \gamma_2). \tag{A24}$$

Then, we conclude that $|\psi_L\rangle$ and $|\psi_R\rangle$ are the edge states. Notably, the existence of the edge modes is independent of the phase diagram arising from the breaking of $\mathcal{T}$ symmetry. The eigenvalues of edge modes are always zero without imaginary part. Similarly, the zero modes of the matrix $h_{CH}^{\dagger}$ can be obtained as

$$\overline{|\psi_L\rangle} = \frac{1}{\sqrt{\Omega}} \sum_{j=1}^{2N} [(\gamma_1)^j - (\gamma_2)^j] \overline{|j_1\rangle}, \tag{A25}$$

$$\overline{|\psi_R\rangle} = \frac{1}{\sqrt{\Omega}} \sum_{j=1}^{2N} [(\gamma_1)^{2N+1-j} - (\gamma_2)^{2N+1-j}] \overline{|j_2\rangle}, \tag{A26}$$

where

$$\overline{|j_1\rangle} = |j\rangle_A - (-1)^j \beta |j\rangle_B, \tag{A27}$$

$$\overline{|j_2\rangle} = |j\rangle_B - (-1)^{2N+1-j} \beta |j\rangle_A. \tag{A28}$$

[1] D. A. McQuarrie, *Quantum Chemistry* (University Science Books, Mill Valley, CA, 1983).

[2] C. M. Bender and S. Boettcher, Real Spectra in Non-Hermitian Hamiltonians Having $\mathcal{PT}$ Symmetry, Phys. Rev. Lett. **80**, 5243 (1998).

[3] C. M. Bender, D. C. Brody, and H. F. Jones, Complex Extension of Quantum Mechanics, Phys. Rev. Lett. **89**, 270401 (2002).

[4] A. Mostafazadeh, Pseudo-Hermiticity versus $\mathcal{PT}$-symmetry: Equivalence of pseudo-Hermiticity and the presence of antilinear symmetries, J. Math. Phys. **43**, 205 (2002).

[5] A. Mostafazadeh, Pseudo-Hermiticity versus $\mathcal{PT}$-symmetry II: Equivalence of pseudo-Hermiticity and the presence of antilinear symmetries, J. Math. Phys. **43**, 2814 (2002).

[6] A. Mostafazadeh, Pseudo-Hermiticity versus $\mathcal{PT}$-symmetry III: Equivalence of pseudo-Hermiticity and the presence of antilinear symmetries, J. Math. Phys. **43**, 3944 (2002).

[7] A. Mostafazadeh, Pseudo-supersymmetric quantum mechanics and isospectral pseudo-Hermitian Hamiltonians, Nucl. Phys. B **640**, 419 (2002).

[8] A. Mostafazadeh, Pseudo-Hermiticity and generalized $\mathcal{PT}$- and $\mathcal{CPT}$-symmetries, J. Math. Phys. **44**, 974 (2003).

[9] L. Jin and Z. Song, Solutions of $\mathcal{PT}$-symmetric tight-binding chain and its equivalent Hermitian counterpart, Phys. Rev. A **80**, 052107 (2009).

[10] L. Jin and Z. Song, Physics counterpart of the $\mathcal{PT}$ non-Hermitian tight-binding chain, Phys. Rev. A **81**, 032109 (2010).

[11] L. Jin and Z. Song, A physical interpretation for the non-Hermitian Hamiltonian, J. Phys. A: Math. Theor. **44**, 375304 (2011).

[12] A. Y. Kitaev, Unpaired Majorana fermions in quantum wires, Phys. Usp. **44**, 131 (2001).

[13] C. Nayak, S. H. Simon, A. Stern, M. Freedman, and S. D. Sarma, Non-Abelian anyons and topological quantum computation, Rev. Mod. Phys. **80**, 1083 (2008).

[14] A. Stern, Non-Abelian states of matter, Nature (London) **464**, 187 (2010).

[15] J. Alicea, New directions in the pursuit of Majorana fermions in solid state systems, Rep. Prog. Phys. **75**, 076501 (2012).

[16] P. Pfeuty, The one-dimensional Ising model with a transverse field, Ann. Phys. **57**, 79 (1970).

[17] S. Sachdev, *Quantum Phase Transitions* (Cambridge University Press, Cambridge, England, 1999).

[18] X. J. Liu, C. L. M. Wong, and K. T. Law, Non-Abelian Majorana Doublets in Time-Reversal-Invariant Topological Superconductors, Phys. Rev. X **4**, 021018 (2014).

[19] X. H. Wang, T. T. Liu, Y. Xiong, and P. Q. Tong, Spontaneous $\mathcal{PT}$-symmetry breaking in non-Hermitian Kitaev and extended Kitaev models, Phys. Rev. A **92**, 012116 (2015).

[20] C. Yuce, Majorana edge modes with gain and loss, Phys. Rev. A **93**, 062130 (2016).

[21] Q. B. Zeng, B. G. Zhu, S. Chen, L. You, and R. Lü, Non-Hermitian Kitaev chain with complex on-site potentials, Phys. Rev. A **94**, 022119 (2016).

[22] M. Klett, H. Cartarius, D. Dast, J. Main, and G. Wunner, Relation between $\mathcal{PT}$-symmetry breaking and topologically nontrivial phases in the Su-Schrieffer-Heeger and Kitaev models, Phys. Rev. A **95**, 053626 (2017).
[23] H. Menke and M. M. Hirschmann, Topological quantum wires with balanced gain and loss, Phys. Rev. B **95**, 174506 (2017).
[24] C. Li, X. Z. Zhang, G. Zhang, and Z. Song, Topological phases in a Kitaev chain with imbalanced pairing, Phys. Rev. B **97**, 115436 (2018).
[25] X. M. Yang and Z. Song, Resonant generation of a -wave Cooper pair in a non-Hermitian Kitaev chain at the exceptional point, Phys. Rev. A **102**, 022219 (2020).
[26] D. Mondal and T. Nag, Anomaly in the dynamical quantum phase transition in a non-Hermitian system with extended gapless phases, Phys. Rev. B **106**, 054308 (2022).
[27] X. Z. Zhang and Z. Song, Non-Hermitian anisotropic XY model with intrinsic rotation-time-reversal symmetry, Phys. Rev. A **87**, 012114 (2013).
[28] C. Li, G. Zhang, X. Z. Zhang, and Z. Song, Conventional quantum phase transition driven by a complex parameter in a non-Hermitian $\mathcal{PT}$-symmetric Ising model, Phys. Rev. A **90**, 012103 (2014).
[29] C. Li and Z. Song, Finite-temperature quantum criticality in a complex-parameter plane, Phys. Rev. A **92**, 062103 (2015).
[30] C. Li, G. Zhang, and Z. Song, Chern number in Ising models with spatially modulated real and complex fields, Phys. Rev. A **94**, 052113 (2016).
[31] M. Franz, Majorana's wires, Nat. Nanotechnol. **8**, 149 (2013).
[32] Y. Ashida, S. Furukawa, and M. Ueda, Parity-time-symmetric quantum critical phenomena, Nat. Commun. **8**, 15791 (2017).
[33] F. D. M. Haldane and S. Raghu, Possible Realization of Directional Optical Waveguides in Photonic Crystals with Broken Time-Reversal Symmetry, Phys. Rev. Lett. **100**, 013904 (2008).
[34] R. Shindou, R. Matsumoto, S. Murakami, and J. Ohe, Topological chiral magnonic edge mode in a magnonic crystal, Phys. Rev. B **87**, 174427 (2013).
[35] R. E. Stanton, Hellmann-Feynman theorem and correlation energies, J. Chem. Phys. **36**, 1298 (1962).
[36] G. Zhang and Z. Song, Topological Characterization of Extended Quantum Ising Models, Phys. Rev. Lett. **115**, 177204 (2015).
[37] D. J. Thouless, *Topological Quantum Numbers in Nonrelativistic Physics* (World Scientific, Singapore, 1998).
[38] M. Z. Hasan and C. L. Kane, Colloquium: Topological insulators, Rev. Mod. Phys. **82**, 3045 (2010).
[39] X.-L. Qi and S.-C. Zhang, Topological insulators and superconductors, Rev. Mod. Phys. **83**, 1057 (2011).
[40] L. Lu, J. D. Joannopoulos, and M. Soljačić, Topological photonics, Nat. Photon. **8**, 821 (2014).
[41] K. Esaki, M. Sato, K. Hasebe, and M. Kohmoto, Edge states and topological phases in non-Hermitian systems, Phys. Rev. B **84**, 205128 (2011).
[42] Y. C. Hu and T. L. Hughes, Absence of topological insulator phases in non-Hermitian $\mathcal{PT}$-symmetric Hamiltonians, Phys. Rev. B **84**, 153101 (2011).
[43] C. M. Bender, Making sense of non-Hermitian Hamiltonians, Rep. Prog. Phys. **70**, 947 (2007).
[44] H. F. Jones, On pseudo-Hermitian Hamiltonians and their Hermitian counterparts, J. Phys. A: Math. Gen. **38**, 1741 (2005).
[45] A. Mostafazadeh, On pseudo-Hermitian Hamiltonians and their Hermitian counterparts, J. Phys. A: Math. Gen. **38**, 6557 (2005).
[46] A. Mostafazadeh, Metric operator in pseudo-Hermitian quantum mechanics and the imaginary cubic potential, J. Phys. A: Math. Gen. **39**, 10171 (2006).
[47] A. Mostafazadeh, Delta-function potential with a complex coupling, J. Phys. A: Math. Gen. **39**, 13495 (2006).
[48] K. L. Zhang and Z. Song, Quantum Phase Transition in a Quantum Ising Chain at Nonzero Temperatures, Phys. Rev. Lett. **126**, 116401 (2021).
[49] K. L. Zhang and Z. Song, Ising chain with topological degeneracy induced by dissipation, Phys. Rev. B **101**, 245152 (2020).
[50] S. Weimann, M. Kremer, Y. Plotnik, Y. Lumer, S. Nolte, K. G. Makris, M. Segev, M. C. Rechtsman, and A. Szameit, Topologically protected bound states in photonic parity-time-symmetric crystals, Nat. Mater. **16**, 433 (2017).
[51] Y. B. Shi, K. L. Zhang, and Z. Song, Dynamic generation of nonequilibrium superconducting states in a Kitaev chain, Phys. Rev. B **106**, 184505 (2022).